ISBN: 978-3-95450-201-1 doi:10.18429/JACoW-IBIC2018-WEPB16

DEVELOPMENT OF A BEAM-GAS CURTAIN PROFILE MONITOR FOR THE HIGH LUMINOSITY UPGRADE OF THE LHC

R. Veness, M. Ady, N. S. Chritin, J. Glutting, T. Marriott-Dodington, O. R. Jones, R. Kersevan, S. Mazzoni, A. Rossi, G. Schneider, CERN, Geneva, Switzerland
P. Forck, S. Udrea, GSI, Darmstadt, Germany
A. Salehilashkajani, C. P. Welsch, H. D. Zhang, Cockcroft Institute and University of Liverpool, Warrington, UK
P. Smakulski, Wrocław University of Science and Technology, Wrocław, Poland

Abstract

High luminosity upgrades to the LHC at CERN and future high-energy frontier machines will require a new generation of minimally invasive profile measurement instruments.

Production of a dense, focussed gas target allows beam-gas fluorescence to be exploited as an observable, giving an instrument suitable for installation even in regions of high magnetic field.

This paper describes the development of a device based on these principles that would be suitable for operation in the LHC. It focusses on mechanisms for the production of a homogeneous gas curtain, the selection of an appropriate working gas and the optical fluorescence detection system.

INTRODUCTION

High-Luminosity LHC (HL-LHC) is under construction as an upgrade to the LHC at CERN [1], planned for commissioning from 2026. The upgrade to the LHC and its injectors will lead to a significant increase in beam intensity. Even the small amount expected to appear as a beam halo will contain significant energy, which must be constantly cleaned to avoid unacceptable losses on the collimation system. The principal technical solution under study for this purpose is a 'hollow electron lens' (HEL) [2] which uses a hollow cylindrical electron beam, constrained by a superconducting solenoid which is passed concentrically around the circulating proton beam over some 3 m of beamline.

Monitoring the concentricity of these two beams during operation will require simultaneous, minimally-invasive, transverse profile measurement of both proton and hollow electron beams. In addition, this measurement must be in close proximity to the solenoid field constraining the electron beam, preventing the collection of charged particles as an observable.

An instrument is being developed to image fluorescence generated by the interaction between these beams and a thin, supersonic, gas curtain [3,4,5]. By tilting this 'Beam Gas Curtain' (BGC) with respect to the beam axis, a 2-D image of both beams can be obtained in much the same way as for a traditional solid screen beam observation system.

The instrument consists of the following main components:

- a gas generation stage consisting of a supersonic gas nozzle followed by three skimmers which select and shape the gas jet.
- an interaction chamber where the 0.45-7 TeV proton beam and 10 keV electron beam interact with the gas jet.
- an optical system for image generation
- an exhaust chamber which pumps the residual gas jet and contains gas jet diagnostics.

There are a number of key developments required for this instrument. It is important to select a working gas that is compatible with the NEG-coated, LHC ultra-high vacuum system, whilst still producing an adequate fluorescence signal from the interaction of both keV electrons and TeV protons, preferably from the spectral line of a neutral atom or molecule to avoid image distortion from electric and magnetic fields. It is also necessary to study the production of a dense supersonic gas curtain whilst minimising the background gas load to the vacuum system, and to develop a radiation-hard imaging system that is efficient for both the electron and proton excited fluorescence signals.

WORKING GASES

As working gases, Nitrogen (N_2) and Neon (Ne) were initially considered [3,6], with estimations made on their cross-sections for relevant transitions at the energies of interest (see Table 2). However, recent considerations regarding vacuum compatibility at CERN lead to the conclusion that N_2 is less desirable than Neon and that a further alternative is Argon (Ar). A literature study was therefore conducted on the fluorescence of Ar and Ar^+ due to excitation by electrons and protons. Whilst a large amount of data is available for fluorescence cross-sections for relatively low-energy ($E_k \leq 1$ keV) electrons impinging on Ar, there is no relevant data for high-energy electrons or protons. According to measurements by [7] for excitation by ≤ 250 eV electrons, the most prominent lines are at 750.4 nm for Ar and 476.5 nm for Ar^+. However, high intensity lines at 751.5 nm (Ar) and 454.5 nm (Ar^+) can also be considered. For extrapolating to higher electron energies the model presented for Ne in [6] has been used for Ar, while for Ar^+ a

ISBN: 978-3-95450-201-1 doi:10.18429/JACoW-IBIC2018-WEPB16

relativistic reformulation of the model from [8,9] has been applied. In both cases data extending to 1 keV from [10] and [11] has also been used. In the case of protons the principle of equal velocities is applied to estimate the cross-sections, i.e. $\sigma_p(7\ \mathrm{TeV}) = \sigma_e(3.8\ \mathrm{GeV})$. The resulting cross-sections are included in Table 2.

OPTICS AND INTEGRATION TIME

Fluorescence cross-sections have to be considered in conjunction with the optical system and the image-intensified camera used for photon detection. A prototype of the set-up to be used on the HEL has been designed and commissioned at GSI [6] and subsequently installed on a test set-up at the Cockcroft Institute, where first tests show promising results. Here we present estimations of the average integration times required for the detection of one photon based on the experience gained and the parameters of Table 1. Note that for working at the large solid angle given in Table 1 a Scheimpflug geometry, see e.g. [12], is envisaged to mitigate issues related to the extremely short depth of field.

The resulting single photon integration times ($\langle t_i \rangle_{MCP}$) for 10 keV electrons and 7 TeV protons are given in Table 2. By multiplying these times with the number of photons needed for a proper image an estimate of the exposure times can be obtained. Considering the small transverse size of the proton beam it is expected that the detection of a few hundred photons should be sufficient to assess its position and shape. The electron beam, however, is distributed over a much larger area, and it is therefore estimated that ~10^4 photons need to be detected for the same purpose. Total integration times of the order of 1 s are thus expected for Ne or Ar as working gases, while in case of N_2 some 10 ms should be adequate. The use of nitrogen, however, has several disadvantages. Firstly, there are compatibility issues with the LHC vacuum system and secondly the relevant emission is only due to the molecular ion. The upper excited level has a relatively long lifetime (60 ns), which may lead to appreciable distortions in the image due to the drift of the ion in the solenoid's magnetic field and strong electromagnetic field of the beams [13].

Table 1: Parameters for Integration Time Estimation

curtain density n	$2.5\cdot10^{10}$ cm^{-3}
curtain thickness d	0.5 mm
optics transmission T	0.85
filter transmission T_f	0.8
solid angle Ω	$40\pi\cdot10^{-4}$ sr
photocathode efficiency η_{pc}	λ-dependent [6]
MCP efficiency η_{MCP}	0.75
average proton current I_p	1 A
DC electron current I_e	5 A

Table 2: Average integration time $\langle t_i \rangle_{MCP}$ for the detection of one emitted photon and total estimated integration time for the three working gases considered, using the parameters defined in Table 1.

Projectile	**Emitter**	**λ [nm]**	**σ [cm²]**	**I [A]**	**η_{pc}**	**Estimated Integration time [s]**	
						Single photon **$\langle t_i \rangle_{MCP}$**	**Total** protons: 10^2 photons electrons: 10^4 photons
electron	N_2^+	391.4	$9.1\cdot10^{-19}$	5	0.19	$2.9\cdot10^{-7}$	0.003
proton	N_2^+	391.4	$3.7\cdot10^{-20}$	1	0.19	$3.6\cdot10^{-5}$	0.004
electron	Ne	585.4	$1.4\cdot10^{-20}$	5	0.09	$4.0\cdot10^{-5}$	0.4
proton	Ne	585.4	$4.7\cdot10^{-22}$	1	0.09	$5.9\cdot10^{-3}$	0.59
electron	Ar	750.4 & 751.5	$7.4\cdot10^{-20}$	5	0.02	$3.4\cdot10^{-5}$	0.34
proton	Ar	750.4 & 751.5	$3.3\cdot10^{-21}$	1	0.02	$3.8\cdot10^{-3}$	0.38
electron	Ar^+	454.5 & 476.5	$9.9\cdot10^{-21}$	5	0.20	$2.5\cdot10^{-5}$	0.25
proton	Ar^+	454.5 & 476.5	$1.7\cdot10^{-21}$	1	0.20	$7.4\cdot10^{-4}$	0.074

GAS JET SIMULATIONS

Formation of the gas stream in the nozzle and subsequent selection and shaping in the skimmers define the gas curtain density at the interaction point with the beam. A predictive design of the BGC gas jet requires simulation of a continuous gas flow with a pressure range of 14 orders of magnitude, from the gas nozzle at 10 bar to the LHC machine vacuum at 10^{-10} mbar.

A hybrid simulation approach to this problem has been taken using Computational Fluid Dynamics (CFD) and Test-Particle Monte Carlo (TPMC). The upstream part, from the supersonic nozzle up to the first skimmer opening,

ISBN: 978-3-95450-201-1 doi:10.18429/JACoW-IBIC2018-WEPB16

has been solved by assuming viscous flow, using CFD. Downstream of the first skimmer a quasi-molecular flow was assumed and the TPMC solver was used. Determination of the transition between the numerical simulation domains was based on the Knudsen number method [14].

Viscous Flow Regime

A set of numerical simulations has been performed in the upstream part in order to maximise the flow rate through the system by maximising the density and axial velocity flow component of the gas before the first skimmer. During the analysis, two nozzle shapes were tested and compared with each other: the 'convergent-divergent' nozzle (CD) and a 'simple geometry' (SG) nozzle with constant diameter. The main parameters under test were the distance between the nozzle throat and the first skimmer opening (see Fig.1), and the nozzle inlet pressure.

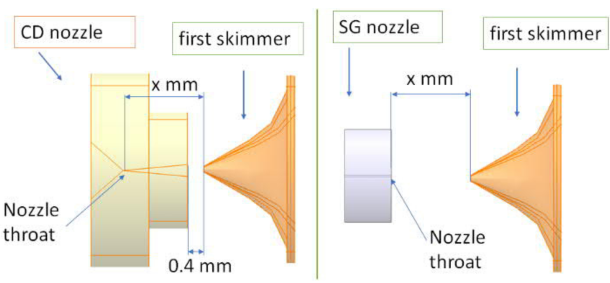

Figure 1: Nozzle and first skimmer as used in the simulations, with x the variable distance between the nozzle throat and the opening of the first skimmer.

For the simulations presented here, the throat diameter of the supersonic nozzle was set to 30 µm. In Fig. 2 the number density and average velocity on the cross-sectional surface of the first skimmer are presented. The simulations show that the CD nozzle gives a significantly better efficiency for gas transport through the first skimmer compared to the SG nozzle. The development of CD nozzles will therefore be prioritised for this project.

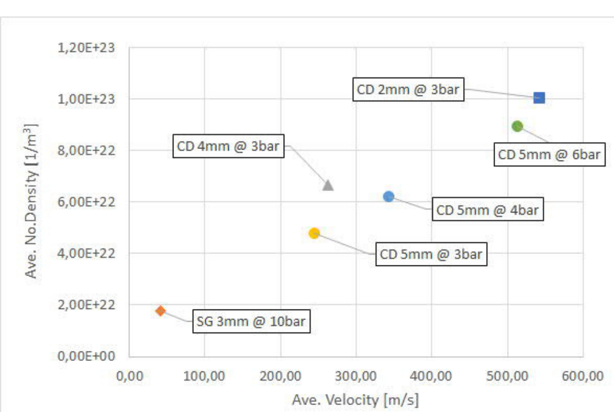

Figure 2: Comparison between nozzle geometries for different nozzle throat to skimmer distances (mm) and inlet pressures (bar).

The flow parameters on the virtual interface of the first skimmer opening were treated as a boundary conditions for the TPMC solver.

All computations were performed using the ANSYS CFX® software and the SST turbulence model. Steady-state calculations for the 2D axis-symmetric numerical domain were iterated until reaching an RMS residual level below 10^{-6}.

Molecular Flow Regime

The low-pressure calculations were performed with the Test-Particle Monte Carlo (TPMC) simulator Molflow+, developed at CERN. A virtual interface at the first skimmer opening was used to generate the gas, so that the flux and direction of particles corresponded to the CFD calculation result at that location. This method predicts an interaction point gas curtain density of $1.2\text{x}10^{10}$ /cm^3, in line with the analytic result in Table 1.

The computed density in all volumes of the system show a well-delimited gas jet in the centre, comprising particles passing the skimmers without any collision, and a background that originates from gas particles bouncing off the skimmers. Simulations suggest the need to pump away these rebounding particles at every skimming stage, to prevent them effusing through the skimmers and increasing the background in the next volume. Every stage therefore has its own pump and a separating cone installed between the volumes (see Fig. 3).

Simulation-led optimisation also suggested the installation of a baffle structure between the beam interaction location and the gas jet exhaust pump. It allows the collimated gas jet to pass through but reduces particle rebound from the tilted turbo-molecular pump (at the end) back to the interaction chamber.

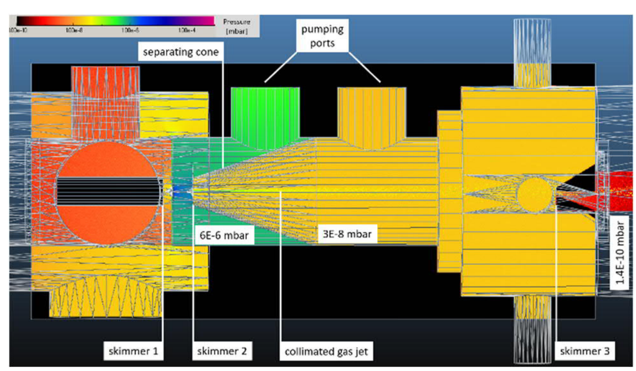

Figure 3: TPMC model showing main components and corresponding pressures.

TESTS IN PROGRESS

A dedicated design of the gas jet system for the LHC environment has been assembled at the Cockcroft Institute [4]. The design incorporates several new aspects to allow for faster component changes and better performance. This includes turbo-molecular pumps with higher pumping speed for a quick pump-down after a vacuum component change, a dedicated interaction chamber, a higher current

ISBN: 978-3-95450-201-1 doi:10.18429/JACoW-IBIC2018-WEPB16

electron-gun to save testing time by reducing the integration time, and an improved imaging system to increase the signal to noise ratio.

Measurements show that a misalignment of only 30 µm in the nozzle and first two skimmers will cause a decrease of 10% in the measurable gas jet signal. The nozzle and first two skimmers have therefore been designed to be aligned in the laboratory using a laser alignment system as a single unit within 30 µm of the ideal axis.

The initial experimental goals for this setup are: to test pumping performance; optimise the gas jet to background pressure ratio; to compare different nozzle and skimmer geometries; to gain operational experience with different candidate gases. Initial tests use a nitrogen gas jet for electron beam profile detection. The next steps will be changing the geometry of the nozzle and skimmer assembly to achieve a higher gas jet density. This system can run in parallel with an older gas jet experiment that was already used to demonstrate the operational principles [6].

DESIGN FOR LHC INSTALLATION

The BGC design must be adapted from the test system set-up at the Cockroft Institute for operation on the LHC (Fig. 4). This poses a number of challenges.

The system must not perturb regular LHC physics operation. It is therefore being designed to be fully isolated from the rest of the machine vacuum system using three all-metal gate valves. When closed, only the interaction chamber will be exposed to the LHC vacuum. This allows the use of positive displacement pumps such as turbo-molecular pumps which have a high pumping speed for inert gases. Beam impedance concerns are addressed by using a copper shielded sleeve with regular slots for vacuum conductance.

The distance between the gas nozzle and interaction point must be compatible with the LHC tunnel dimensions. In addition, the final instrument will be required to fit into the 200 mm longitudinal gap between the HEL solenoid cryostats.

The background pressure in the interaction chamber must be as low as possible. The volume between each skimmer as well as the interaction and exhaust chambers will therefore be pumped separately. In total five volumes will require positive displacement pumps. The final number of pumps could be reduced by sharing backing pumps and using only a primary pump between the nozzle and first skimmer.

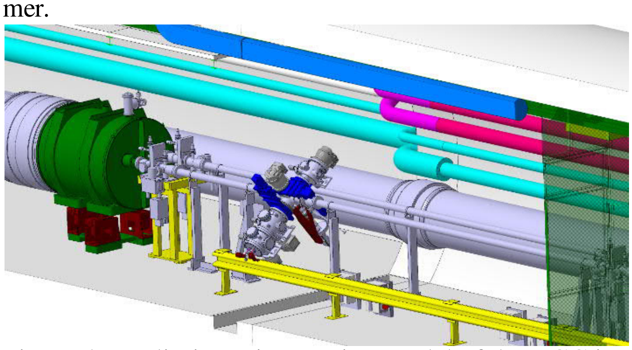

Figure 4 : Preliminary integration model of the BGC instrument in the LHC

STATUS AND NEXT STEPS

Neon is currently the gas species which seems to provide the best balance of integration time, low excited-state lifetime and vacuum compatibility for use in this application, with Argon as a useful fall-back solution. Simulations show that a practical optical system design can deliver a useable signal with such gases within a matter of seconds.

Viscous and molecular flow simulations have been combined to produce a working tool for optimisation of the gas jet system and associated LHC vacuum components.

Tests are in progress with a newly designed experimental bench to validate the gas selection, optics and gas jet geometry. In parallel, design and integration of an instrument for installation in the LHC is in progress.

A test set-up is also currently installed in the LHC to verify the fluorescence predictions based on the theoretically estimated cross-sections and to assess the background due to the LHC environment. The next step will be to test a prototype instrument both on high-intensity electron beams and in the LHC.

ACKNOWLEDGEMENTS

The authors would like to thank The Hi Lumi project and the Science and Technology Facilities Council of the UK for supporting this project via a CERN collaboration agreement. Thanks also to Ahmed Cherif from CERN EN-MME for nozzle production support.

REFERENCES

[1] http://hilumilhc.web.cern.ch/

[2] S.Redaelli *et al.* "Plans for deployment of hollow electron lenses at the LHC for enhanced beam collimation" in *Proc. IPAC'15*, Richmond, VA, USA, paper WEBB1.

[3] S. Udrea, *et al.*, "Preparatory Work for a Fluorescence based Profile Monitor for an Electron Lens", in *Proc. IBIC'16*, Barcelona, Spain, September 2016, paper TUPG73, p. 528.

[4] H.D. Zhang et al., "A supersonic gas jet-based beam profile monitor using flourescence for HL-LHC", in *Proc. IPAC'18*, Vancouver, BC, Canada. Doi:10.18429/JACoW-IPAC2018-WEBPAF034

[5] V.Tzoganis et al., "A non-invasive beam profile monitor for charged particle beams", *Applied Physics Letters,* vol. 104 (20), p. 204104, 2014

[6] S. Udrea *et al.*, "Development of a Fluorescence based Gas Sheet Profile Monitor for use with Electron Lenses: Optical System Design and Preparatory Experiments", in *Proc. IBIC'17*, Grand Rapids, MI, USA, August 2017, paper WEPCC08, p. 359.

[7] J.B. Boffard, B. Chiaro, T. Weber, and C.C. Lin, "Electron-Impact Excitation of Argon: Optical Emission Cross Sections in the Range of 300–2500 nm", *Atom. Dat. and Nucl. Dat. Tables*, vol. 93, p. 831, 2007.

[8] J.M. Ajello, G.K. James, B.O. Franklin, and D.E. Shemansky, "Medium-Resolution Studies of Extreme Ultraviolet Emission from N_2 by Electron Impact: Vibrational Perturbations and Cross Sections of the c'$_4$ $^1\Sigma_u^+$ and b' $^1\Sigma_g^+$ States", *Phys. Rev. A.*, vol. 40, p. 3524, 1989.

ISBN: 978-3-95450-201-1 doi:10.18429/JACoW-IBIC2018-WEPB16

[9] D.E. Shemansky, J.M. Ajello, D.T. Hall, and B. Franklin, "Vacuum Ultraviolet Studies of Electron Impact of Helium: Excitation of He n^1P_o Rydberg Series and Ionization-Excitation of He^+ nl Rydberg Series", *The Astrophys. J.*, vol. 296, p. 774, 1985.

[10] S. Tsurubuchi, T. Miyazaki, and K. Motohashi, "Electron-impact emission cross sections of Ar*", J. Phys. B: At. Mol. Opt. Phys.*, vol. 29, p. 1785, 1996.

[11] S. Tsurubuchi, "Emission Cross Sections of Ar^+ Measured in a Wide Range of Electron Impact Energies", *J. Phys. Soc. Japan*, vol. 66, p. 3070, 1997.

[12] Ch. Wiebers *et al.*, "Scintillating Screen Monitors for Transverse Electron Beam Profile Diagnostics at the European XFEL", in *Proc. IBIC'13,* Oxford, UK, September 2013, paper WEPF03, p. 807.

[13] D. Vilsmeier, P. Forck, M. Sapinski, "A modular Application for IPM Simulations", in *Proc. IBIC'17*, Grand Rapids, MI, USA, August 2017, paper WEPCC07, p. 355.

[14] La F. Torre, S. Kenjereš, J-L. Moerel and C.R. Kleijn, "Hybrid simulations of rarefied supersonic gas flows in micro-nozzles", *Comput. Fluids* 49 (2011) 312–22